nanomaterials

MDPI

Article

The Role of Temperature on the Degree of End-Closing and Filling of Single-Walled Carbon Nanotubes

Magdalena Kierkowicz [1], Elzbieta Pach [2], Julio Fraile [1], Concepción Domingo [1], Belén Ballesteros [2] and Gerard Tobias [1,*]

[1] Institut de Ciència de Materials de Barcelona (ICMAB-CSIC), Campus UAB, Bellaterra, 08193 Barcelona, Spain; mkierkowicz@gmail.com (M.K.); julio@icmab.es (J.F.); conchi@icmab.es (C.D.)
[2] Catalan Institute of Nanoscience and Nanotechnology (ICN2), CSIC and the Barcelona Institute of Science and Technology, Campus UAB, Bellaterra, 08193 Barcelona, Spain; epach@icmab.es (E.P.); belen.ballesteros@icn2.cat (B.B.)
* Correspondence: gerard.tobias@icmab.es

Abstract: Carbon nanotubes (CNTs), owing to their high surface area-to-volume ratio and hollow core, can be employed as hosts for adsorbed and/or encapsulated molecules. At high temperatures, the ends of CNTs close spontaneously, which is relevant for several applications, including catalysis, gas storage, and biomedical imaging and therapy. This study highlights the influence of the annealing temperature in the range between 400 and 1100 °C on the structure and morphology of single-walled CNTs. The nitrogen adsorption and density functional theory calculations indicate that the fraction of end-closed CNTs increases with temperature. Raman spectroscopy reveals that the thermal treatment does not alter the tubular structure. Insight is also provided into the efficacy of CNTs filling from the molten phase, depending on the annealing temperature. The CNTs are filled with europium (III) chloride and analyzed by using electron microscopy (scanning electron microscopy and high-resolution transmission electron microscopy) and energy-dispersive X-ray spectroscopy, confirming the presence of filling and closed ends. The filling yield increases with temperature, as determined by thermogravimetric analysis. The obtained results show that the apparent surface area of CNTs, fraction of closed ends, and amount of encapsulated payload can be tailored via annealing.

Keywords: carbon nanocapsules; filled carbon nanotubes; end-closing; encapsulation; sealing

Citation: Kierkowicz, M.; Pach, E.; Fraile, J.; Domingo, C.; Ballesteros, B.; Tobias, G. The Role of Temperature on the Degree of End-Closing and Filling of Single-Walled Carbon Nanotubes. *Nanomaterials* **2021**, *11*, 3365. https://doi.org/10.3390/nano11123365

Academic Editors: Marianna V. Kharlamova, Christian Kramberger and Alexander Chernov

Received: 5 November 2021
Accepted: 2 December 2021
Published: 11 December 2021

1. Introduction

Single-walled carbon nanotubes (SWCNTs) are cylindrical nanostructures composed of individual rolled-up carbon sp^2 sheets arranged as adjacent hexagons. As-produced SWCNTs are usually closed with hemifullerene caps. The diameter ranges between 0.7 and 3 nm, depending on the method of synthesis. Owing to their high surface area-to-volume ratio, SWCNTs have strong potential for water purification, drug delivery, tissue engineering, catalysis, sensors, and photovoltaics to name some of their applications [1–5]. Different molecules and particles can be attached onto their external surface or inside the tubular channels, thus expanding their functionality.

There is a special interest in using SWCNTs as enclosures for the encapsulation of payloads [6–9]. The nanotubes offer protection to the hosted material from the external environment, thus allowing, for instance, the encapsulation of air sensitive materials [10], gases [11], and even radionuclides [12,13]. Furthermore, a large variety of unprecedented structures have been observed by confinement of materials at the nanoscale [14]. Filled SWCNTs find applications in diverse areas, including nanoelectronics, magnetic recording, nanobiotechnology, sensors, spintronics, catalysis, energy storage, and thermoelectrics [15]. Bulk filling of SWCNTs in general results in samples containing unwanted material external to the nanotube walls. The presence of external material can dominate the properties of the resulting hybrids and can also induce side effects when employed in the biomedical field.

Unless the encapsulated payloads have a strong interaction with the inner nanotube walls, it is necessary to seal/block the ends of the SWCNTs to allow for the selective removal of the non-encapsulated compounds while preserving the inner cargo [16]. SWCNTs can be filled with a chosen payload by using different methods, the most commonly employed being solution phase, molten phase, and sublimation. When the filling process takes place at a high enough temperature, typically a few hundred degrees Celsius, spontaneous closure of the ends of CNTs occurs simultaneously [17]. Fullerenes can also be used to block the ends of both SWCNTs [18,19] and multi-walled CNTs (MWCNTs) [20] in the low-temperature methods. However, this process can be reversible, since the removal of fullerene corks can be triggered by changes in the solvent [19] and pH when the fullerenes are functionalized [21]. Filled and closed-ended CNTs can be referred to as "carbon nanocapsules" [22] because the walls of the nanotubes provide protection to the encapsulated cargo [23].

Closed- and opened-end CNTs have different textural properties that can be monitored by low-temperature N_2 adsorption [24–27]. The Brunauer–Emmett–Teller (BET) theory is used here for the calculation of the apparent specific surface area of CNTs [28,29]. CNTs tend to form bundles owing to Van der Waals interactions. Therefore, the potential surfaces available for gas adsorption on SWCNTs include the outer area, inner channels (mainly micropores), interstitial channels, and grooves [30,31], as schematically illustrated in Figure S1 (see Supporting Information). Studies comparing the adsorption from a liquid and gaseous phase in CNTs prove that the outer and inner surfaces of the isolated tubes play the most important role in adsorption [32]. Moreover, the presence of impurities, amorphous carbon, and functional groups may reduce the adsorption capacity of CNTs [33]. Therefore, a thermal treatment is sometimes required to restore the storage capacity of CNTs. For instance, annealing is widely used to recover and improve the performance of CNT-based catalysts and sensors [34,35]. However, it should be taken into account that when a sufficiently high temperature is achieved, CNTs end-closure takes place, and their internal cavity is no longer accessible for adsorption. It has been shown that closed-cap nanotubes exhibit high current stability, which is of advantage for their use as electron sources [36]. While the end-closure of SWCNTs by thermal annealing is known to occur [37], the fraction of capped ends at different temperatures, and the consequent implications for filling, remain to be explored.

Herein, we perform a systematic study to understand the role of temperature on the degree of end-closing of SWCNTs and filling yield when carbon nanotubes are filled with $EuCl_3$ by molten phase capillary wetting. Europium–CNT hybrids have received attention due to the luminescent properties that europium confers to the system [38–40].

2. Materials and Methods

Chemical vapor deposition (CVD)-grown SWCNTs (Elicarb®, Thomas Swan & Co. Ltd., Consett, UK) contained a mixture of both single-walled (SWCNTs) and double-walled CNTs (DWCNTs). For ease of description, this mixture has been referred to as SWCNTs throughout the manuscript. According to the supplier, the average diameter of the CNTs was 2.1 nm. Iron catalyst particles surrounded by graphitic shells, graphitic particles and amorphous carbon were also present in the sample. Therefore, previous to any processing, CNTs were purified and open-ended with water steam (4 h) and hydrochloric acid (HCl) reflux (6 h), based on a method described in previous studies [41]. This method was employed because no damage to the tubular structure has been reported even after prolonged treatments [42]. Steam reacts through the ends of the carbon nanotubes, preserving the sp^2 backbone. For each study, the same batch of purified CNTs was used. One batch of purified CNTs (250 mg) was split into five equal fractions. Each sample (50 mg) was sealed in a silica tube under vacuum. One sample was directly opened at room temperature (RT), with no thermal treatment, and referred to as RT-CNTs. The rest of the ampoules, containing the samples under vacuum, were heated at 300 °C min^{-1} in a furnace for 12 h at the selected temperatures of 400, 700, 900, and 1100 °C. After the thermal treatment the ampoules were opened on a laboratory bench (in air).

A second batch of purified CNTs was used for filling with a molten salt. For this, purified and open-ended CNTs were mixed with $EuCl_3$ (europium (III) chloride anhydrous, 99.99%, Darmstadt, Alemania) in a weight ratio of 1:10, and then ground using an agate mortar and pestle inside an argon-filled glovebox (Labconco, Kansas City, MO, USA). The sample was split into four equal fractions (125 mg each). Each fraction was introduced into an individual silica tube and sealed under vacuum. The filling experiment was performed using the same program and temperature values as those applied for empty CNTs. After the thermal treatment the ampoules were opened on a laboratory bench (in air). The $EuCl_3$-filled CNTs ($EuCl_3$@CNTs) contained some unencapsulated material that was removed by extensive washing with hot water.

TGA (Q5000 IR) was performed in air using a heating ramp of 10 °C min^{-1} and up to 900 °C.

Raman spectra were recorded using a LabRam HR8000 (Jobin-Yvon, Palaiseau, France) Raman spectrometer with an excitation wavelength of 532 nm (Ar laser, 10% power). A 100× objective was used in this study. The abscissa was calibrated using a silicon standard. Samples were deposited from an isopropanol dispersion as thin films on glass microscopy slides. The reported I_D/I_G values corresponded to the average of three measurements registered for the same sample at different spots (three accumulations per spot, accumulation time of 5 s). The spectra were normalized to the intensity of the G band.

Nitrogen adsorption isotherms were measured at the temperature of liquid nitrogen (−196 °C) using an ASAP-2020 Micromeritics equipment. Before adsorption, the samples were degassed at 300 °C for 12 h.

High-angle annular dark-field scanning transmission electron microscopy (HAADF-STEM) images were acquired by using scanning electron microscopy (SEM; FEI Magellan XHR) at 20 kV with STEM. High resolution transmission electron microscopy (HRTEM) images were obtained by using FEI Tecnai G2 F20 at 200 kV. Elemental mapping of the sample was performed using an EDAX super ultra-thin window X-ray detector coupled to the Tecnai HRTEM. All samples were drop cast from the dispersion in anhydrous ethanol on lacey carbon Cu grids (Agar Scientific, Stansted, UK).

3. Results and Discussion

The as-received, purified (RT) and annealed (at 400, 700, 900, and 1100 °C) empty SWCNTs were studied by conducting low-temperature nitrogen adsorption tests. The apparent specific surface area (S_{BET}) was determined by applying the BET method (Figure 1a). Pore size distribution of the different samples was computed using a model based on nonlocal density functional theory (NLDFT). To estimate the cumulative pore volume (V_C), only the pores in the range of 0.3–1.5 nm were considered. This range was chosen by observing the representation of the NLDFT differential pore volume vs. pore width (Figure 1b). Actually, this range of pore diameters is in agreement with the diameters of the SWCNTs used (containing a fraction of DWCNTs), previously determined by employing Raman spectroscopy and high-resolution transmission electron microscopy (HRTEM) [43]. As expected, the size of the pores is smaller than the actual diameter of the nanotubes. The values were also consistent with the information provided by the manufacturer.

Figure 1 and Table S1 (see Supporting Information) show that the as-received CNTs have a significantly lower S_{BET} and V_C than purified SWCNTs (RT). This result shows that the steam treatment efficiently opens the ends of the SWCNTs and removes carbonaceous impurities, thereby significantly increasing the accessible S_{BET} from 791 in as-received to 1246 m^2 g^{-1} in RT-CNTs and V_C from 0.146 to 0.231 cm^3 g^{-1}. The high values of these textural properties were largely retained by annealing up to temperatures of 700 °C. However, annealing of purified CNTs at 900 °C and above resulted in a progressive decrease in S_{BET} and V_C, although this reduction was less pronounced than the increase observed between the as-received and purified RT-CNTs. This observation indicates that at 900 °C, the ends of the CNTs started to close, and the fraction of the end-closed CNTs increased as a function of temperature.

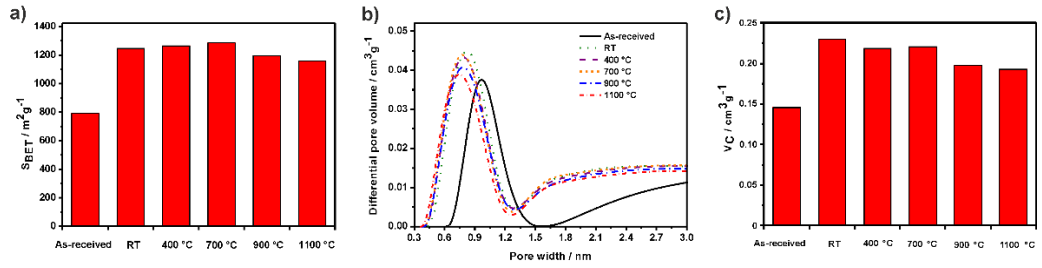

Figure 1. (**a**) Histogram representing the apparent specific surface area (S_{BET}), (**b**) nonlocal density functional theory (NLDFT) pore size distribution, and (**c**) histogram of cumulative volume (V_C) for as−received, purified (RT) and annealed SWCNTs (at 400, 700, 900, and 1100 °C).

Raman spectroscopy did not reveal any significant differences between the purified CNTs (RT) and the thermally treated samples. The I_D/I_G values (Figure 2) were similar in all cases and remained between 0.11 and 0.14 (Table S2; see Supporting Information), indicating that annealing in this range of temperatures did not significantly alter the tubular structure of CNTs. Taking into account the aspect ratio of the employed carbon nanotubes, the I_D/I_G values do not provide information on whether the ends of the nanotubes are opened or closed.

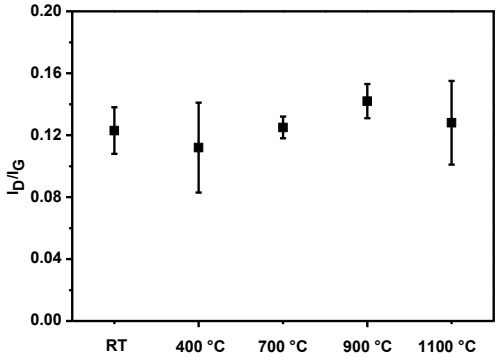

Figure 2. I_D/I_G values extracted from Raman spectra of purified (RT) and annealed SWCNTs (at 400, 700, 900, and 1100 °C). Each value is the average of three measurements. SWCNTs were excited using a laser wavelength of 532 nm.

Thermogravimetric analysis (TGA) of the empty and filled SWCNTs was performed under air flow. Figure 3a shows the influence of annealing at selected temperatures on the empty purified CNTs. Compared with the as-received, both the purified (RT) and all the samples of annealed SWCNTs exhibit higher thermal stability against oxidation by air. This is because the steam and HCl treatment removes both carbonaceous impurities and metal catalyst from the sample. The carbonaceous impurities present mainly consist of amorphous carbon and graphitic particles [44]. The presence of such carbonaceous impurities is responsible for the initial weight loss observed at 300–400 °C in the TGA of the as-received SWCNTs, which can be better appreciated in the inset of Figure 3a. The amorphous carbon is much more reactive with oxygen and oxidizes first. The inorganic solid residue collected after the complete combustion of the as-received SWCNTs was 4.6 wt.%. After purification, it decreased to approximately 1.3 wt.%, and remained at this value after the thermal treatment, within experimental error. The as-received sample has a lower combustion temperature than the purified SWCNTs (RT) due to the presence of the carbonaceous impurities in the former. The metal catalyst might also play a role, because samples containing higher concentrations of metal impurities showed a decrease in the temperature required to oxidize the sample [45].

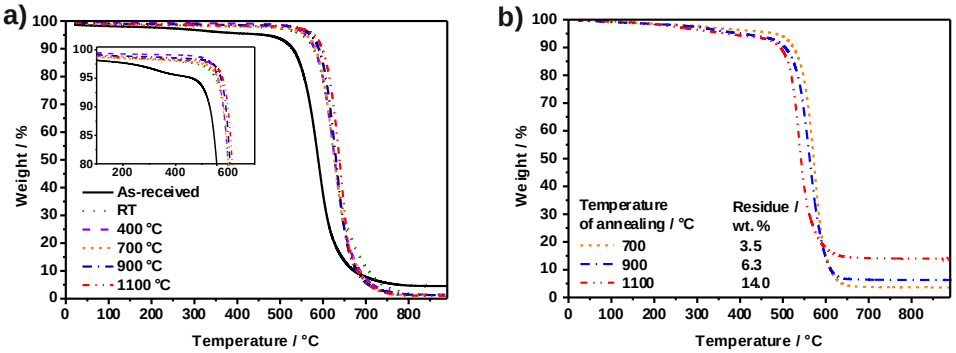

Figure 3. Thermogravimetric analyses of: (**a**) as-received, purified (RT) and annealed SWCNTs (at 400, 700, 900, and 1100 °C); and (**b**) SWCNTs filled with $EuCl_3$ at selected temperatures. Measurements were performed under air flow.

Next, three temperatures (700, 900, and 1100 °C) were employed for the melt filling of purified CNTs with $EuCl_3$. The resulting samples were independently washed to remove $EuCl_3$ that remained on the exterior of the CNTs [46]. The amount of $EuCl_3$ encapsulated after the filling experiment at each temperature was estimated from TGA measurements performed under flowing air (Figure 3b). For $EuCl_3$@CNTs samples, carbon oxidizes first, and the remaining residues corresponded to Eu_2O_3 formed by oxidation of the metal halide. The formula reported by Ballesteros et al. [47] was used to calculate the amount of encapsulated payload ($EuCl_3$) from the TGA residue of each sample. The filling yields turned out to be 3.1, 7.3 and 19.3 wt.% for samples treated at 700, 900 and 1100 °C, respectively. As can be observed, the amount of inorganic residue after the TGA analyses increased with the temperature used in the filling process. Hence, the sample obtained at the highest temperature was characterized by the highest filling yield. Based on these results, it is shown that the filling yield is temperature-dependent, and the amount of encapsulated payload can be controlled by controlling the melt temperature. The higher filling yield obtained at higher temperatures is correlated with the fraction of CNTs with closed ends, i.e., the highest being the number of CNTs having closed ends, the lowest being the probability of washing-out of the encapsulated payload. Nevertheless, it could also be the case that by increasing the temperature used for the filling experiment, $EuCl_3$ more easily enters the cavities of CNTs. Temperature plays a key role in filling CNTs; thermal cycles have been previously employed to achieve a high filling yield [48], and it is also known that the temperature of the melt determines the crystal structure of the resulting confined material, for instance, from nanowires to van der Waals heterostructures [49].

After the filling and washing processes, the CNTs were characterized by using electron microscopy. HAADF-STEM was initially employed to assess the overall filling of the sample (Figure 4a). In this imaging modality, the intensity offered by an element is proportional to its atomic number. Therefore, carbon appears as pale gray and the encapsulated material, containing europium, as bright lines following the shape of the carbon nanotube bundles. There are several bright lines corresponding to the filling material. The small bright particles correspond to filling, of either CNTs or graphitic particles, in the form of nanoparticles or to catalytic particles that remain after the purification step. Bundle crossing also results in higher intensity. HRTEM was employed to confirm the absence of non-encapsulated europium chloride, to examine the crystalline structure of the filling, and the condition of the ends after the filling experiment at 1100 °C (Figure 4b and Figure S2; see Supporting Information). As it can be seen in the images, carbon nanotubes are irregularly shaped graphitic particles were found to be filled. The image in Figure 4b shows bundles of CNTs containing both filled and empty nanotubes and some visible closed ends. The presence of empty nanotubes was observed in all the samples. Therefore, it is better to employ TGA to assess the loading efficiency [47]. As a guide to the eye, white arrows point to CNTs filled with nanowires of $EuCl_3$, empty white arrows to filling with nanoparticles, and black

arrows point to closed ends. Having closed ends prevents leakage of the payload during the washing steps. Notably, during HRTEM analysis a single-layered inorganic nanotube of $EuCl_3$ was found inside the cavities of a large diameter DWCNT (see Supporting Information Figure S2b), thus creating a tubular (1 D) van der Waals heterostructure, as previously observed for other encapsulated 2D materials [50–54]. TEM imaging combined with EDX spectroscopy confirmed the presence of $EuCl_3$ in the internal cavity of the CNTs (Figure 4c). Europium and chlorine peaks are clearly visible in the EDX spectrum. The copper peaks arise from the support grid.

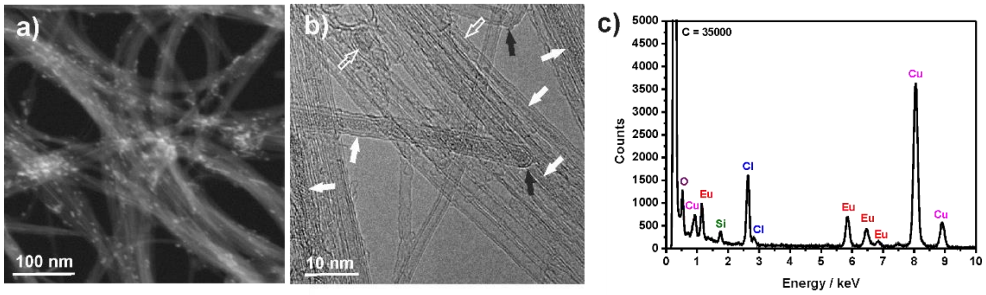

Figure 4. Electron microscopy imaging and energy-dispersive X-ray (EDX) spectroscopy of $EuCl_3$@CNTs filled at 1100 °C. (**a**) High-angle annular dark-field scanning transmission electron microscopy (HAADF-STEM) image, (**b**) High resolution transmission electron microscopy (HRTEM) image (as a guide to the eye, white arrows point to CNTs filled with nanowires of $EuCl_3$, empty white arrows to filling with nanoparticles, and black arrows point to closed ends) and (**c**) EDX spectrum of the sample, confirming the presence of Eu and Cl (the carbon peak maxima was cut down for better visibility of lower intensity peaks).

It is worth noting that the end-closing of SWCNTs takes place at lower temperatures than MWCNTs [16], and therefore it is a diameter dependent process. It has also been reported that in the case of MWCNTs, the number of walls also plays a role in the degree of end-closing [36]. This is important because whereas the SWNCTs employed in this study have an average diameter of 2.1 nm, SWCNTs from other sources such as arc-discharge, or HiPco typically have smaller diameters. Therefore, lower temperatures than those employed in the present study might be enough to efficiently close the ends of the nanotubes and render a high filling yield.

4. Conclusions

The effect of temperature on the degree of end-closing and filling of SWCNTs has been investigated. Low-temperature nitrogen adsorption tests showed that the S_{BET} and Vc of the CNTs increased after purification and decreased by annealing in the temperature range of 900–1100 °C, which is associated with the progressive closure of the ends of the CNTs. Electron microscopy and TGA analysis indicate that annealing did not affect the purity and structure of the CNTs. Using $EuCl_3$@CNTs, it was demonstrated that increasing the annealing temperature had a positive effect on the filling yield from the molten phase, which was found to be correlated with the fraction of CNTs with closed ends. In summary, the fraction of end-closed CNTs and the filling yield can be tuned by controlling the annealing temperature.

Supplementary Materials: The following are available online at https://www.mdpi.com/article/10.3390/nano11123365/s1, Table S1: Apparent specific surface area (S_{BET}) and cumulative pore volume (V_C), Table S2: I_D/I_G Raman ratios, Figure S1: Schematic representation of gas adsorption in a bundle of SWCNTs, Figure S2: Additional HRTEM images.

Author Contributions: Conceptualization, G.T.; methodology, M.K.; investigation, M.K., E.P., J.F.; writing—original draft preparation, M.K. and E.P.; writing—review and editing, J.F., C.D., B.B., G.T.; supervision, C.D., B.B., G.T.; funding acquisition, C.D., B.B., G.T. All authors have read and agreed to the published version of the manuscript.

Funding: The research leading to these results has received funding from the Ministerio de Ciencia e Innovación (Spain) through the grants ECIME (PID2020-113805GB-I00 and PID2020-115631GB-I00) and from FP7 ITN project RADDEL (290023). ICMAB and ICN2 acknowledge financial support from the Spanish Ministry of Economy and Competitiveness, through the "Severo Ochoa" Programme for Centres of Excellence in R&D (CEX2019-000917-S and SEV-2017-0706 respectively). The APC was funded by CSIC and PID2020-113805GB-I00. ICN2 is funded by the CERCA programme/Generalitat de Catalunya.

Institutional Review Board Statement: Not applicable.

Informed Consent Statement: Not applicable.

Data Availability Statement: Not applicable.

Acknowledgments: The authors are grateful to Thomas Swan & Co. Ltd. (Consett, UK) for providing Elicarb® SWCNTs.

Conflicts of Interest: The authors declare no conflict of interest.

References

1. Dubey, R.; Dutta, D.; Sarkar, A.; Chattopadhyay, P. Functionalized carbon nanotubes: Synthesis, properties and applications in water purification, drug delivery, and material and biomedical sciences. *Nanoscale Adv.* **2021**, *3*, 5722–5744. [CrossRef]
2. Barrejón, M.; Marchesan, S.; Alegret, N.; Prato, M. Carbon nanotubes for cardiac tissue regeneration: State of the art and perspectives. *Carbon* **2021**, *184*, 641–650. [CrossRef]
3. Kumari, A.; Rajeev, R.; Benny, L.; Sudhakar, Y.N.; Varghese, A.; Hegde, G. Recent advances in carbon nanotubes-based biocatalysts and their applications. *Adv. Colloid Interface Sci.* **2021**, *297*, 102542. [CrossRef] [PubMed]
4. Speranza, G. Carbon Nanomaterials: Synthesis, Functionalization and Sensing Applications. *Nanomaterials* **2021**, *11*, 967. [CrossRef]
5. Mao, B.; Hodges, B.; Franklin, C.; Calatayud, D.G.; Pascu, S.I. Self-Assembled Materials Incorporating Functional Porphyrins and Carbon Nanoplatforms as Building Blocks for Photovoltaic Energy Applications. *Front. Chem.* **2021**, *9*, 696. [CrossRef] [PubMed]
6. Kashtiban, R.J.; Burdanova, M.G.; Vasylenko, A.; Wynn, J.; Medeiros, P.V.C.; Ramasse, Q.; Morris, A.J.; Quigley, D.; Lloyd-Hughes, J.; Sloan, J. Linear and Helical Cesium Iodide Atomic Chains in Ultranarrow Single-Walled Carbon Nanotubes: Impact on Optical Properties. *ACS Nano* **2021**, *15*, 13389–13398. [CrossRef] [PubMed]
7. Del Carmen Giménez-López, M.; Moro, F.; La Torre, A.; Gómez-García, C.J.; Brown, P.D.; Van Slageren, J.; Khlobystov, A.N. Encapsulation of single-molecule magnets in carbon nanotubes. *Nat. Commun.* **2011**, *2*, 1–6. [CrossRef]
8. Kharlamova, M.V. Nickelocene-filled purely metallic single-walled carbon nanotubes: Sorting and tuning the electronic properties. *Nanomaterials* **2021**, *11*, 2500. [CrossRef]
9. Kharlamova, M.V.; Kramberger, C. Metal Cluster Size-Dependent Activation Energies of Growth of Single-Chirality Single-Walled Carbon Nanotubes inside Metallocene-Filled Single-Walled Carbon Nanotubes. *Nanomaterials* **2021**, *11*, 2649. [CrossRef]
10. Hart, M.; Chen, J.; Michaelides, A.; Sella, A.; Shaffer, M.S.P.; Salzmann, C.G. One-Dimensional Pnictogen Allotropes inside Single-Wall Carbon Nanotubes. *Inorg. Chem.* **2019**, *58*, 15216–15224. [CrossRef]
11. Serpell, C.J.; Rutte, R.N.; Geraki, K.; Pach, E.; Martincic, M.; Kierkowicz, M.; De Munari, S.; Wals, K.; Raj, R.; Ballesteros, B.; et al. Carbon nanotubes allow capture of krypton, barium and lead for multichannel biological X-ray fluorescence imaging. *Nat. Commun.* **2016**, *7*, 13118. [CrossRef]
12. Wang, J.T.W.; Klippstein, R.; Martincic, M.; Pach, E.; Feldman, R.; Šefl, M.; Michel, Y.; Asker, D.; Sosabowski, J.K.; Kalbac, M.; et al. Neutron Activated ^{153}Sm Sealed in Carbon Nanocapsules for in Vivo Imaging and Tumor Radiotherapy. *ACS Nano* **2020**, *14*, 129–141. [CrossRef]
13. Ge, H.; Riss, P.J.; Mirabello, V.; Calatayud, D.G.; Flower, S.E.; Arrowsmith, R.L.; Fryer, T.D.; Hong, Y.; Sawiak, S.; Jacobs, R.M.J.; et al. Behavior of Supramolecular Assemblies of Radiometal-Filled and Fluorescent Carbon Nanocapsules In Vitro and In Vivo. *Chem* **2017**, *3*, 437–460. [CrossRef]
14. Sandoval, S.; Tobias, G.; Flahaut, E. Structure of inorganic nanocrystals confined within carbon nanotubes. *Inorg. Chim. Acta* **2019**, *492*, 66–75. [CrossRef]
15. Kharlamova, M.V.; Kramberger, C. Applications of Filled Single-Walled Carbon Nanotubes: Progress, Challenges, and Perspectives. *Nanomaterials* **2021**, *11*, 2863. [CrossRef] [PubMed]
16. Martincic, M.; Vranic, S.; Pach, E.; Sandoval, S.; Ballesteros, B.; Kostarelos, K.; Tobias, G. Non-cytotoxic carbon nanocapsules synthesized via one-pot filling and end-closing of multi-walled carbon nanotubes. *Carbon* **2019**, *141*, 782–793. [CrossRef]

17. Shao, L.; Tobias, G.; Huh, Y.; Green, M.L.H. Reversible filling of single walled carbon nanotubes opened by alkali hydroxides. *Carbon* **2006**, *44*, 2855–2858. [CrossRef]
18. Shao, L.; Lin, T.W.; Tobias, G.; Green, M.L.H. A simple method for the containment and purification of filled open-ended single wall carbon nanotubes using C60 molecules. *Chem. Commun.* **2008**, *18*, 2164–2166. [CrossRef]
19. Ren, Y.; Pastorin, G. Incorporation of Hexamethylmelamine inside Capped Carbon Nanotubes. *Adv. Mater.* **2008**, *20*, 2031–2036. [CrossRef]
20. Sandoval, S.; Tobias, G. Encapsulation of Fullerenes: A Versatile Approach for the Confinement and Release of Materials Within Open-Ended Multiwalled Carbon Nanotubes. *Front. Bioeng. Biotechnol.* **2021**, *9*, 644793. [CrossRef]
21. Luksirikul, P.; Ballesteros, B.; Tobias, G.; Moloney, M.G.; Green, M.L.H. pH-triggered release of materials from single-walled carbon nanotubes using dimethylamino-functionalized fullerenes as removable "corks". *Carbon* **2010**, *48*, 1912–1917. [CrossRef]
22. Tobias, G.; Ballesteros, B.; Ballesteros, B. Carbon nanocapsules: Blocking materials inside carbon nanotubes. *Phys. Status Solidi. C Curr. Top. Solid State Phys.* **2010**, *7*, 2739–2742. [CrossRef]
23. Serpell, C.J.; Kostarelos, K.; Davis, B.G. Can Carbon Nanotubes Deliver on Their Promise in Biology? Harnessing Unique Properties for Unparalleled Applications. *ACS Cent. Sci.* **2016**, *2*, 190–200. [CrossRef]
24. Agnihotri, S.; Rostam Abadi, M.; Rood, M. Temporal changes in nitrogen adsorption properties of single-walled carbon nanotubes. *Carbon* **2004**, *42*, 2699–2710. [CrossRef]
25. Furmaniak, S.; Terzyk, A.; Gauden, P.; Gauden, P.A.; Wisniewski, M.; Wiśniewski, M.; Kowalczyk, P. Simple model of adsorption on external surface of carbon nanotubes—a new analytical approach basing on molecular simulation data. *Adsorption* **2010**, *16*, 197–213. [CrossRef]
26. Byl, O.; Liu, J.; Yates Jr, J.T. Characterization of single wall carbon nanotubes by nonane preadsorption. *Carbon* **2006**, *44*, 2039–2044. [CrossRef]
27. Arai, M.; Kanamaru, M.; Matsumura, T.; Hattori, Y.; Utsumi, S.; Ohba, T.; Tanaka, H.; Yang, C.M.; Kanoh, H.; Okino, F.; et al. Pore characterization of assembly-structure controlled single wall carbon nanotube. *Adsorption* **2007**, *13*, 509–514. [CrossRef]
28. Maryam, M.; Suriani, A.B.; Shamsudin, M.S.; Rusop, M. BET Analysis on Carbon Nanotubes: Comparison Between Single and Double Stage Thermal CVD Method. *Adv. Mater. Res.* **2013**, *626*, 289–293. [CrossRef]
29. Birch, M.E.; Ruda-Eberenz, T.A.; Chai, M.; Andrews, R.; Hatfield, R.L. Properties that Influence the Specific Surface Areas of Carbon Nanotubes and Nanofibers. *Ann. Occup. Hyg.* **2013**, *57*, 1148–1166. [CrossRef] [PubMed]
30. Ren, X.; Chen, C.; Nagatsu, M.; Wang, X. Carbon nanotubes as adsorbents in environmental pollution management: A review. *Chem. Eng. J.* **2011**, *170*, 395–410. [CrossRef]
31. Rawat, D.S.; Calbi, M.M.; Migone, A.D. Equilibration Time: Kinetics of Gas Adsorption on Closed- and Open-Ended Single-Walled Carbon Nanotubes. *J. Phys. Chem. C* **2007**, *111*, 12980–12986. [CrossRef]
32. Wiśniewski, M.; Gauden, P.A.; Terzyk, A.P.; Kowalczyk, P.; Pacholczyk, A.; Furmaniak, S. Detecting adsorption space in carbon nanotubes by benzene uptake. *J. Colloid Interface Sci.* **2013**, *391*, 74–85. [CrossRef] [PubMed]
33. Lafi, L.; Cossement, D.; Chahine, R. Raman spectroscopy and nitrogen vapour adsorption for the study of structural changes during purification of single-wall carbon nanotubes. *Carbon* **2005**, *43*, 1347–1357. [CrossRef]
34. Kocabas, S.; Kopac, T.; Dogu, G.; Dogu, T. Effect of thermal treatments and palladium loading on hydrogen sorption characteristics of single-walled carbon nanotubes. *Int. J. Hydrog. Energy* **2008**, *33*, 1693–1699. [CrossRef]
35. Yu, L.F.a.A.M. Carbon Nanotubes Based Thin Films: Fabrication, Characterization and Applications. *Rev. Adv. Mater. Sci.* **2014**, *36*, 40–61.
36. De Jonge, N.; Doytcheva, M.; Allioux, M.; Kaiser, M.; Mentink, S.A.M.; Teo, K.B.K.; Lacerda, R.G.; Milne, W.I. Cap Closing of Thin Carbon Nanotubes. *Adv. Mater.* **2005**, *17*, 451–455. [CrossRef]
37. Geng, H.Z.; Zhang, X.B.; Mao, S.H.; Kleinhammes, A.; Shimoda, H.; Wu, Y.; Zhou, O. Opening and closing of single-wall carbon nanotubes. *Chem. Phys. Lett.* **2004**, *399*, 109–113. [CrossRef]
38. Avti, P.K.; Sitharaman, B. Luminescent single-walled carbon nanotube-sensitized europium nanoprobes for cellular imaging. *Int. J. Nanomed.* **2012**, *7*, 1953–1964. [CrossRef]
39. Wu, D.; Xin, X.; Pang, X.; Pietraszkiewicz, M.; Hozyst, R.; Sun, X.; Wei, Q. Application of Europium Multiwalled Carbon Nanotubes as Novel Luminophores in an Electrochemiluminescent Aptasensor for Thrombin Using Multiple Amplification Strategies. *ACS Appl. Mater. Interfaces* **2015**, *7*, 12663–12670. [CrossRef] [PubMed]
40. Sitharaman, B.; Rajamani, S.; Avti, P.K. Time-resolved red luminescence from europium-catalyzed single walled carbon nanotubes. *Chem. Commun.* **2011**, *47*, 1607–1609. [CrossRef]
41. Tobias, G.; Shao, L.; Salzmann, C.G.; Huh, Y.; Green, M.L.H. Purification and Opening of Carbon Nanotubes Using Steam. *J. Phys. Chem. B* **2006**, *110*, 22318–22322. [CrossRef]
42. Ballesteros, B.; Tobias, G.; Shao, L.; Pellicer, E.; Nogués, J.; Mendoza, E.; Green, M.L.H. Steam Purification for the Removal of Graphitic Shells Coating Catalytic Particles and the Shortening of Single-Walled Carbon Nanotubes. *Small* **2008**, *4*, 1501–1506. [CrossRef]
43. Kierkowicz, M.; Pach, E.; Santidrián, A.; Tobías-Rossell, E.; Kalbáč, M.; Ballesteros, B.; Tobias, G. Effect of Steam-Treatment Time on the Length and Structure of Single-Walled and Double-Walled Carbon Nanotubes. *ChemNanoMat* **2016**, *2*, 108–116. [CrossRef]
44. Cabana, L.; Ke, X.; Kepić, D.; Oro-Solé, J.; Tobías-Rossell, E.; Van Tendeloo, G.; Tobias, G. The role of steam treatment on the structure, purity and length distribution of multi-walled carbon nanotubes. *Carbon* **2015**, *93*, 1059–1067. [CrossRef]

45. Hernández-Rivera, M.; Kumar, I.; Cho, S.Y.; Cheong, B.Y.; Pulikkathara, M.X.; Moghaddam, S.E.; Whitmire, K.H.; Wilson, L.J. High-Performance Hybrid Bismuth–Carbon Nanotube Based Contrast Agent for X-ray CT Imaging. *ACS Appl. Mater. Interfaces* **2017**, *9*, 5709–5716. [CrossRef]
46. Martincic, M.; Pach, E.; Ballesteros, B.; Tobias, G. Quantitative monitoring of the removal of non-encapsulated material external to filled carbon nanotube samples. *Phys. Chem. Chem. Phys.* **2015**, *17*, 31662–31669. [CrossRef]
47. Ballesteros, B.n.; Tobias, G.; Ward, M.A.H.; Green, M.L.H. Quantitative Assessment of the Amount of Material Encapsulated in Filled Carbon Nanotubes. *J. Phys. Chem. C* **2009**, *113*, 2653–2656. [CrossRef]
48. Brown, G.; Bailey, S.R.; Novotny, M.; Carter, R.; Flahaut, E.; Coleman, K.S.; Hutchison, J.L.; Green, M.L.H.; Sloan, J. High yield incorporation and washing properties of halides incorporated into single walled carbon nanotubes. *Appl. Phys. A* **2003**, *76*, 457–462. [CrossRef]
49. Sandoval, S.; Pach, E.; Ballesteros, B.; Tobias, G. Encapsulation of two-dimensional materials inside carbon nanotubes: Towards an enhanced synthesis of single-layered metal halides. *Carbon* **2017**, *123*, 129–134. [CrossRef]
50. Cabana, L.; Ballesteros, B.; Batista, E.; Magén, C.; Arenal, R.; Oró-Solé, J.; Rurali, R.; Tobias, G. Synthesis of PbI_2 Single-Layered Inorganic Nanotubes Encapsulated Within Carbon Nanotubes. *Adv. Mater.* **2014**, *26*, 2016–2021. [CrossRef]
51. Sandoval, S.; Kepić, D.; Pérez del Pino, Á.; György, E.; Gómez, A.; Pfannmoeller, M.; Tendeloo, G.V.; Ballesteros, B.; Tobias, G. Selective Laser-Assisted Synthesis of Tubular van der Waals Heterostructures of Single-Layered PbI_2 within Carbon Nanotubes Exhibiting Carrier Photogeneration. *ACS Nano* **2018**, *12*, 6648–6656. [CrossRef] [PubMed]
52. Serra, M.; Arenal, R.; Tenne, R. An overview of the recent advances in inorganic nanotubes. *Nanoscale* **2019**, *11*, 8073–8090. [CrossRef] [PubMed]
53. Sinha, S.S.; Sreedhara, M.B.; Tenne, R. Why do nanocrystals of 2D materials form nanotubes and why is that important? *Nano Today* **2021**, *37*, 101060. [CrossRef]
54. Zheng, Y.; Kumamoto, A.; Hisama, K.; Otsuka, K.; Wickerson, G.; Sato, Y.; Liu, M.; Inoue, T.; Chiashi, S.; Tang, D.-M.; et al. One-dimensional van der Waals heterostructures: Growth mechanism and handedness correlation revealed by nondestructive TEM. *Proc. Natl. Acad. Sci. USA* **2021**, *118*, e2107295118. [CrossRef]